Aerotecnica Missili & Spazio
https://doi.org/10.1007/s42496-025-00266-4

RESEARCH

Free Vibrations of Composite Cylindrical Panels with Cutouts of General Shape

Marco Lo Cascio[1] · **Alberto Milazzo**[1]

Received: 14 February 2025 / Revised: 27 March 2025 / Accepted: 28 March 2025

Abstract
A novel single-domain Ritz method is presented for analyzing the free vibrations of laminated cylindrical panels with cutouts of general shape. The structural model of the panel is based on the first-order shear deformation theory. In this framework, the primary variables—midplane displacements and section rotations—are represented using trial functions, constructed as tensor products of one-dimensional orthogonal Legendre polynomials. The governing equations are derived by enforcing the stationarity of the total potential energy. This leads to a standard eigenvalue problem, the solution of which yields the panel's free vibration frequencies and modes. To compute the matrices involved in the governing equations, a specialized integration approach is employed, which leverages an implicit cutout representation via level set functions, ensuring accurate integral evaluation over the panel domain. A series of validation results showcasing the method's accuracy and ability to handle various configurations, including different boundary conditions, laminate layups, cutout geometries and positions, are proposed to demonstrate the effectiveness of the proposed method.

Keywords Composite shells · Cutouts · Free-vibration analysis · Ritz method

1 Introduction

Composite laminated cylindrical shells/panels are widely used in aerospace applications due to their unique properties, such as high strength and stiffness-to-weight ratios. Their potential for tailored structural performance resulting from innovative design and optimisation strategies further enhances their versatility. These structural components are frequently subjected to dynamic loads, which can generate strain and stress fields that exceed predictions from static analyses, particularly when the natural frequencies of the structure are excited [1, 2]. Consequently, it is essential to conduct thorough investigations of their dynamic behavior, and a significant amount of research has focused on developing accurate and efficient methods for assessing their vibration characteristics. Moreover, composite laminated cylindrical shells/panels feature cutout openings, such as windows, holes, and access cutouts, to meet functional and weight requirements, adding complexity to their behavior and modeling.

Composite laminated shells have been the subject of significant research interest for many years and extensive literature on this subject can be found in many review articles and books [3–7].

Composite laminated cylindrical shells/panels often incorporate cutout openings to meet functional and weight requirements, adding complexity to their behavior and modeling. The free vibration behavior of composite laminated shells with cutouts has been studied using different approaches. Bicos and Springer [8] presented a first-order theory-based finite element solution for the vibration characteristics of laminated cylindrical shells with circular cutouts, including the damping effect. Sahu and Datta [9] used an FSDT-based finite element model with an eight-noded isoparametric shell element to study the vibration and buckling of composite curved panels with cutouts. Nanda and Bandyopadhyay [10] used eight-noded C0 continuity, isoparametric quadrilateral finite elements to model the nonlinear free vibration of laminated composite cylindrical shell panels with cutouts. Chaubey et al. [11] presented a C0 finite element formulation based on third-order shear

✉ Alberto Milazzo
alberto.milazzo@unipa.it

Marco Lo Cascio
marco.locascio01@unipa.it

[1] Department of Engineering, Universitá degli Studi di Palermo, Viale delle Scienze, Bldg 8, 90135 Palermo, Italy

Published online: 02 May 2025

deformation theory (TSDT) to study the free vibration analysis of composite cylindrical shells with cutouts. Poore et al. [12] developed a semi-analytical solution method to study the influences of various geometrical parameters on the vibration behavior of laminated cylindrical shells containing a circular cutout. Dey et al. [13] performed stochastic natural frequency analyses based on a support vector regression (SVR) model of laminated composite curved panels with cutouts. Kurpa et al. [14] used the R-functions method based on the FSDT to study the geometric nonlinear vibration response of laminated shallow shells with central rectangular clamped cutouts. Kwak et al. [15] proposed an FSDT-based meshless method using the Tchebychev-radial point interpolation shape function to analyze the free vibration characteristics of laminated closed conical, cylindrical shells, and annular plates. Talezadehlari [16] investigated the free vibration behavior of composite cylindrical shells with a central square cutout using the multi-domain Generalized Differential Quadrature (GDQ) method.

The Ritz method [17] is a numerical technique that is renowned for its computational efficiency. It has been extensively employed to analyze the linear [18, 19] and nonlinear vibrations [20, 21] of laminated cylindrical shells and the influence of boundary conditions [22–24], fiber orientation [25, 26], embedded cracks [27], and complex geometries [28–31].

Within the Ritz method framework, the present work proposes a novel single-domain formulation for modeling the free vibrations of cylindrical laminated composite shells with cutouts. The structural model is based on the first-order shear deformation theory (FSDT), whose primary variables, namely the shell midplane translation and the shell section rotations, are approximated by a set of trial functions built with orthogonal Legendre polynomials. The resolving algebraic system is obtained by applying the stationarity condition of the total potential energy. This results in a system of equations involving the unknown Ritz coefficients associated with the primary variables. The characteristic matrices of this system are computed using a unique integration technique, which employs an implicit description of the cutout via an appropriately defined level set function. This technique allows an accurate evaluation of domain integrals over the shell domain and is the core and main novelty of the proposed Ritz approach. Validation results and studies are provided to demonstrate the effectiveness and potential of this method.

2 Formulation

Let us consider a cylindrical shell panel with rectangular planform, having radius R, panel open angle 2α and length $2L$ as depicted in Fig. 1a. It is built as a laminate with general layup having N_L constant thickness layers of composite material. The panel is constrained along its external edges and it presents a cutout of general shape and position whose edges are free.

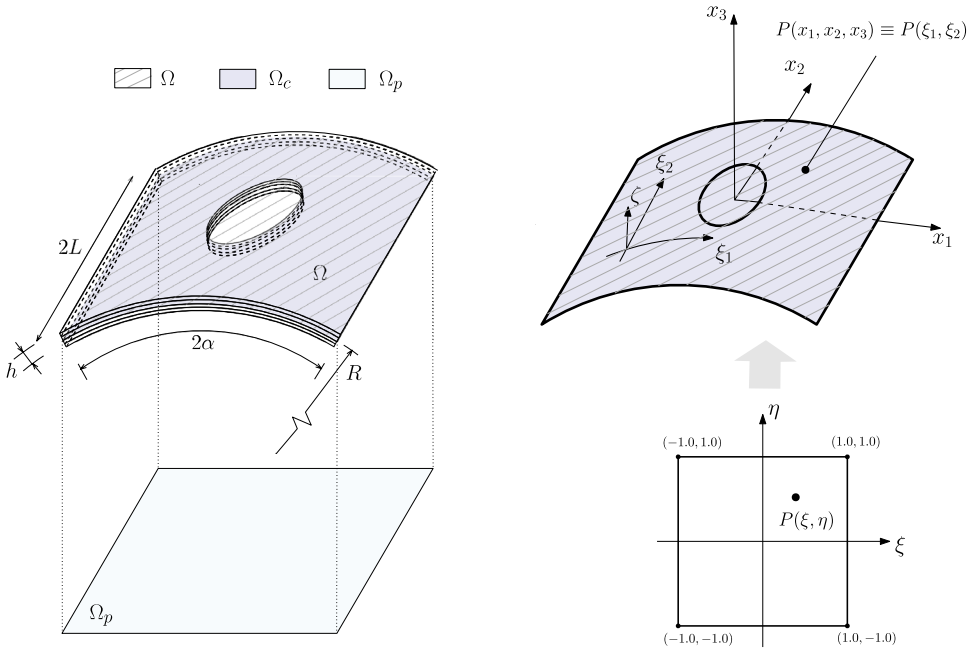

(a) Geometry.

(b) Reference systems and mapping.

Fig. 1 Cylindrical panel geometry and reference systems

2.1 Panel Geometry Description

The panel is geometrically defined by its mid-surface, which occupies the domain Ω with boundary $\partial\Omega$. This mid-surface is described using a Cartesian coordinate system, where the x_1 and x_2 axes span the rectangular planform domain Ω_p, with the origin located at the center of the planform. A curvilinear orthogonal coordinate system ξ_1, ξ_2, ζ is then defined on the mid-surface, where ξ_1 aligns with the circumferential direction, ξ_2 is parallel to the cylinder axis, and ζ is oriented normal to the panel's mid-surface. Finally, a linear mapping is established between the curvilinear coordinates ξ_1 and ξ_2 which span the domain Ω and the natural coordinates ξ and η, which span the domain $Q \equiv [-1,1]\times[-1,1]$. Figure 1b illustrates the reference systems used and, based on these, the coordinates of a point on the panel's mid-surface are given by

$$\begin{Bmatrix} x_1 \\ x_2 \\ x_3 \end{Bmatrix} = \begin{Bmatrix} R\sin\frac{\xi_1}{R} \\ \xi_2 \\ R\left(\cos\frac{\xi_1}{R} - \cos\alpha\right) \end{Bmatrix} = \begin{Bmatrix} R\sin\alpha\xi \\ L\eta \\ R(\cos\alpha\xi - \cos\alpha) \end{Bmatrix} \tag{1}$$

2.2 Cutout Geometry Description

The panel can present a cutout obtained by intersecting it with a general cylindrical section whose axis is aligned with the x_3 direction, as illustrated in Fig. 2a.

The geometry of the cutout is implicitly defined using a *level set* function φ, expressed in terms of Cartesian coordinates x_1 and x_2, such that $\varphi = \varphi(\boldsymbol{P}) = \varphi(x_1, x_2)$. Based on this definition, the mid-surface domain of the cutted panel, denoted as Ω_c, is the region of Ω where the function φ takes negative values (see Fig. 2b):

$$\Omega_c \equiv \{(x_1, x_2, x_3) \in \Omega \ : \ \varphi(x_1, x_2) < 0\}. \tag{2}$$

Similarly, the boundary of the cutout, Γ, corresponds to the set of Ω points where φ equals zero:

$$\Gamma \equiv \{(x_1, x_2, x_3) \in \Omega \ : \ \varphi(x_1, x_2) = 0\}. \tag{3}$$

It is worth noting that if there is no cut, Ω_c equals Ω. The *level set* function φ can also be expressed in terms of the curvilinear coordinates $\xi_1\ \xi_2\ \zeta$ or the natural coordinates $\xi\ \eta$ using Eq. (1). Examples of cutout shapes and the associated *level set* functions are provided in Appendix 7.

2.3 Shell Panel Kinematics

The panel structural model is based on the first-order shear deformation theory (FSDT) and the displacement field is assumed as

$$\boldsymbol{d} = \boldsymbol{u} + \zeta\, \boldsymbol{L}\boldsymbol{\vartheta} \tag{4}$$

where $\boldsymbol{d} = \left\{d_{\xi_1}\ \ d_{\xi_2}\ \ d_\zeta\right\}^T$ is the displacement vector containing the displacement components along the ξ_1, ξ_2 and ζ axes, and

$$\boldsymbol{L} = \begin{bmatrix} 1 & 0 & 0 \\ 0 & 1 & 0 \end{bmatrix}^T \tag{5}$$

In Eq. (4), the generalized displacement vectors $\boldsymbol{u}$ and $\boldsymbol{\vartheta}$ are defined as $\boldsymbol{u} = \left\{u\ v\ w\right\}^T$ and $\boldsymbol{\vartheta} = \left\{\vartheta_{\xi_1}\ \ \vartheta_{\xi_2}\right\}^T$ being u and v the in-plane translations of the mid-surface points along the ξ_1 and ξ_2 axes, w the transverse deflection along the ζ direction, ϑ_{ξ_1} and ϑ_{ξ_2} the section rotations around the ξ_2 and ξ_1-axis, respectively.

The strain field is suitably partitioned into the in-plane and out-of-plane components collected into the vectors

Fig. 2 Cutout definition

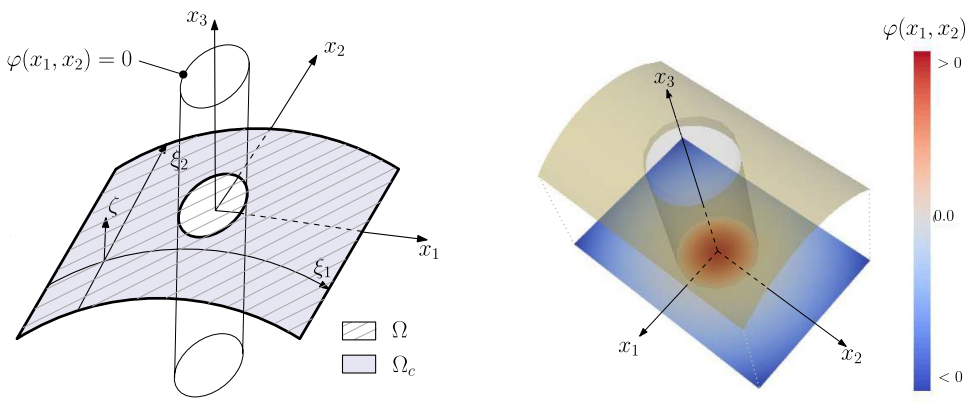

(a) Geometry. (b) Level set function.

$\boldsymbol{e}_p = \left\{e_{11}\ e_{22}\ e_{12}\right\}^T$ and $\boldsymbol{e}_n = \left\{e_{13}\ e_{23}\right\}^T$, respectively. By introducing the thickness operators

$$\boldsymbol{Z} = \begin{bmatrix} \frac{1}{(1+\zeta/R)} & 0 & 0 & 0 \\ 0 & 1 & 0 & 0 \\ 0 & 0 & \frac{1}{(1+\zeta/R)} & 1 \end{bmatrix} \tag{6a}$$

$$\boldsymbol{Z}_S = \begin{bmatrix} \frac{1}{(1+\zeta/R)} & 0 \\ 0 & 1 \end{bmatrix} \tag{6b}$$

the linear strain–displacement relations are written as [32]

$$\boldsymbol{e}_p = \boldsymbol{Z}\boldsymbol{\varepsilon} + \zeta\boldsymbol{Z}\boldsymbol{\kappa} \tag{7a}$$

$$\boldsymbol{e}_n = \boldsymbol{Z}_S\boldsymbol{\gamma} \tag{7b}$$

where the generalized strain vectors $\boldsymbol{\varepsilon}$,$\boldsymbol{\kappa}$ and $\boldsymbol{\gamma}$ are defined as

$$\boldsymbol{\varepsilon} = \begin{bmatrix} \frac{\partial}{\partial\xi_1} & 0 & \frac{1}{R} \\ 0 & \frac{\partial}{\partial\xi_2} & 0 \\ 0 & \frac{\partial}{\partial\xi_1} & 0 \\ \frac{\partial}{\partial\xi_2} & 0 & 0 \end{bmatrix} \begin{Bmatrix} u \\ v \\ w \end{Bmatrix} = \mathscr{D}_{pu}\boldsymbol{u} \tag{8a}$$

$$\boldsymbol{\kappa} = \begin{bmatrix} \frac{\partial}{\partial\xi_1} & 0 \\ 0 & \frac{\partial}{\partial\xi_2} \\ 0 & \frac{\partial}{\partial\xi_1} \\ \frac{\partial}{\partial\xi_2} & 0 \end{bmatrix} \begin{Bmatrix} \vartheta_{\xi_1} \\ \vartheta_{\xi_2} \end{Bmatrix} = \mathscr{D}_{p\vartheta}\boldsymbol{\vartheta} \tag{8b}$$

$$\boldsymbol{\gamma} = \begin{Bmatrix} \vartheta_{\xi_1} \\ \vartheta_{\xi_2} \end{Bmatrix} + \begin{bmatrix} -\frac{1}{R} & 0 & \frac{\partial}{\partial\xi_1} \\ 0 & 0 & \frac{\partial}{\partial\xi_2} \end{bmatrix} \begin{Bmatrix} u \\ v \\ w \end{Bmatrix} = \boldsymbol{\vartheta} + \mathscr{D}_{nu}\boldsymbol{u} \tag{8c}$$

2.4 Ply Constitutive Equations

Assuming plane stress condition ($\sigma_{33} = 0$), the k-th ply constitutive equations are written as

$$\begin{Bmatrix} \boldsymbol{\sigma}_p^{\langle k\rangle} \\ \boldsymbol{\sigma}_n^{\langle k\rangle} \end{Bmatrix} = \begin{Bmatrix} \sigma_{11}^{\langle k\rangle} \\ \sigma_{22}^{\langle k\rangle} \\ \sigma_{12}^{\langle k\rangle} \\ \hline \sigma_{31}^{\langle k\rangle} \\ \sigma_{32}^{\langle k\rangle} \end{Bmatrix} = \begin{bmatrix} \boldsymbol{Q}_p^{\langle k\rangle} & \boldsymbol{0} \\ \boldsymbol{0} & \boldsymbol{Q}_n^{\langle k\rangle} \end{bmatrix} \begin{Bmatrix} \boldsymbol{e}_p \\ \boldsymbol{e}_n \end{Bmatrix} \tag{9}$$

where the superscript $\langle k\rangle$ is employed to denote quantities related to the k-th ply. The elements of the ply stiffness matrices $\boldsymbol{Q}_p^{\langle k\rangle}$ and $\boldsymbol{Q}_n^{\langle k\rangle}$ have the following expressions

$$Q_{p11}^{\langle k\rangle} = \bar{Q}_{11}^{\langle k\rangle}\cos^4\theta + 2\left(\bar{Q}_{12}^{\langle k\rangle} + 2\bar{Q}_{33}^{\langle k\rangle}\right)\sin^2\theta\cos^2\theta + \bar{Q}_{22}^{\langle k\rangle}\sin^4\theta \tag{10a}$$

$$Q_{p12^{\langle k\rangle}} = \bar{Q}_{12}^{\langle k\rangle}\cos^4\theta + \left(\bar{Q}_{11}^{\langle k\rangle} + Q_{22}^{\langle k\rangle} - 4\bar{Q}_{33}^{\langle k\rangle}\right)\sin^2\theta\cos^2\theta + \bar{Q}_{12}^{\langle k\rangle}\sin^4\theta \tag{10b}$$

$$Q_{p22}^{\langle k\rangle} = \bar{Q}_{11}^{\langle k\rangle}\sin^4\theta + 2\left(\bar{Q}_{12}^{\langle k\rangle} + 2\bar{Q}_{33}^{\langle k\rangle}\right)\sin^2\theta\cos^2\theta + \bar{Q}_{22}^{\langle k\rangle}\cos^4\theta \tag{10c}$$

$$Q_{p13}^{\langle k\rangle} = \left(\bar{Q}_{11}^{\langle k\rangle} - Q_{12}^{\langle k\rangle} - 2\bar{Q}_{33}^{\langle k\rangle}\right)\sin\theta\cos^3\theta + \left(\bar{Q}_{12}^{\langle k\rangle} - Q_{22}^{\langle k\rangle} + 2\bar{Q}_{33}^{\langle k\rangle}\right)\sin^3\theta\cos\theta \tag{10d}$$

$$Q_{p23}^{\langle k\rangle} = \left(\bar{Q}_{11}^{\langle k\rangle} - Q_{12}^{\langle k\rangle} - 2\bar{Q}_{33}^{\langle k\rangle}\right)\sin^3\theta\cos\theta + \left(\bar{Q}_{12}^{\langle k\rangle} - Q_{22}^{\langle k\rangle} + 2\bar{Q}_{33}^{\langle k\rangle}\right)\sin\theta\cos^3\theta \tag{10e}$$

$$Q_{p33}^{\langle k\rangle} = \left(\bar{Q}_{11}^{\langle k\rangle} + Q_{22}^{\langle k\rangle} - 2\bar{Q}_{12}^{\langle k\rangle} - 2\bar{Q}_{66}^{\langle k\rangle}\right)\sin^2\theta\cos^2\theta + \bar{Q}_{33}^{\langle k\rangle}\left(\sin^4\theta + \cos^4\theta\right)\cos\theta \tag{10f}$$

$$Q_{n11}^{\langle k\rangle} = \bar{Q}_{44}^{\langle k\rangle}\cos^2\theta + \bar{Q}_{55}^{\langle k\rangle}\sin^2\theta \tag{10g}$$

$$Q_{n12} = \left(\bar{Q}_{55}^{\langle k\rangle} - \bar{Q}_{44}^{\langle k\rangle}\right)\cos\theta\sin\theta \tag{10h}$$

$$Q_{n22}^{\langle k\rangle} = \bar{Q}_{44}^{\langle k\rangle}\sin^2\theta + \bar{Q}_{55}^{\langle k\rangle}\cos^2\theta \tag{10i}$$

where θ is the stacking angle, measured with respect to the ξ_1-axis, and

$$\bar{Q}_{11} = \frac{E_1}{1-\nu_{12}\nu_{21}} \tag{11a}$$

$$\bar{Q}_{22} = \frac{E_2}{1-\nu_{12}\nu_{21}} \tag{11b}$$

$$\bar{Q}_{12} = \frac{\nu_{12}E_2}{1-\nu_{12}\nu_{21}} \tag{11c}$$

$$\bar{Q}_{66} = G_{12} \tag{11d}$$

$$\bar{Q}_{44} = G_{23} \tag{11e}$$

$$\bar{Q}_{44} = G_{13} \tag{11f}$$

being E_i the Young's moduli, G_{ij} the shear moduli and ν_{ij} the Poisson' coefficients in the material orthotropic reference system.

2.5 Equilibrium and Governing Equation for the Free Vibration Problem

The equilibrium governing equations for the free vibration problem are derived from the stationarity conditions of the energy potential, assuming that the kinematical boundary conditions of the problem are satisfied [33]. The energy potential is expressed as follows:

$$\begin{aligned}\Pi = &\int_{\Omega_c} \sum_{k=1}^{N_L} \int_{h_{k-1}}^{h_k} \frac{1}{2}\left[\boldsymbol{e}_p^T \boldsymbol{Q}_p^{\langle k\rangle} \boldsymbol{e}_p + \boldsymbol{e}_n^T \boldsymbol{Q}_n^{\langle k\rangle} \boldsymbol{e}_n^{\langle k\rangle}\right](1 + k_1\bar{\zeta})(1 + k_2\bar{\zeta})\mathrm{d}\zeta\,\mathrm{d}\Omega \\ &- \omega^2 \int_{\Omega_c} \sum_{k=1}^{N_L} \int_{h_{k-1}}^{h_k} \frac{1}{2}\rho^{\langle k\rangle} \mathbf{d}^T \mathbf{d}(1 + k_1\bar{\zeta})(1 + k_2\bar{\zeta})\mathrm{d}\zeta\,\mathrm{d}\Omega\end{aligned} \tag{12}$$

where ω represents the circular frequency of vibration, h_{k-1} and h_k denote the ζ coordinates of the bottom and top faces of the k-th ply, and $\rho^{\langle k\rangle}$ is the density of the k-th ply. Accounting for the kinematics and ply constitutive equations and integrating over the panel thickness, the energy potential can be written as

$$\begin{aligned}\Pi = &\int_{\Omega_c} \frac{1}{2}\left[\boldsymbol{\varepsilon}^T \boldsymbol{A}\,\boldsymbol{\varepsilon} + \boldsymbol{\varepsilon}^T \boldsymbol{B}\,\boldsymbol{\kappa} + \boldsymbol{\kappa}^T \boldsymbol{B}\,\boldsymbol{\varepsilon} + \boldsymbol{\kappa}^T \boldsymbol{D}\,\boldsymbol{\kappa} + \boldsymbol{\gamma}^T \boldsymbol{A}_S\,\boldsymbol{\gamma}\right]\mathrm{d}\Omega - \\ &\omega^2 \int_{\Omega_c} \frac{1}{2}\left[\boldsymbol{u}^T \boldsymbol{I}_{uu}\boldsymbol{u} + \boldsymbol{u}^T \boldsymbol{I}_{u\vartheta}\boldsymbol{\vartheta} + \boldsymbol{\vartheta}^T \boldsymbol{I}_{\vartheta u}\boldsymbol{u} + \boldsymbol{\vartheta}^T \boldsymbol{I}_{\vartheta\vartheta}\boldsymbol{\vartheta}\right]\mathrm{d}\Omega\end{aligned} \tag{13}$$

where the panel stiffness and inertia matrices are defined as

$$\langle \boldsymbol{A}, \boldsymbol{B}, \boldsymbol{D}\rangle = \sum_{k=1}^{N_L} \int_{h_{k-1}}^{h_k} \boldsymbol{Z}^T \boldsymbol{Q}_p^{\langle k\rangle} \langle 1, \zeta, \zeta^2\rangle \boldsymbol{Z}(1 + \zeta/R)\mathrm{d}\zeta \tag{14a}$$

$$\boldsymbol{A}_S = \sum_{k=1}^{N_L} \int_{h_{k-1}}^{h_k} \boldsymbol{Z}_S^T \boldsymbol{Q}_s^{\langle k\rangle} \boldsymbol{Z}_S\,(1 + \zeta/R)\mathrm{d}\zeta \tag{14b}$$

$$\langle \boldsymbol{I}_{uu}, \boldsymbol{I}_{u\vartheta}, \boldsymbol{I}_{\vartheta u}, \boldsymbol{I}_{\vartheta\vartheta}\rangle = \sum_{k=1}^{N_L} \int_{h_{k-1}}^{h_k} \rho^{\langle k\rangle} \langle \boldsymbol{I}_{3\times 3}, \zeta\boldsymbol{L}, \zeta\boldsymbol{L}^T, \zeta^2\boldsymbol{L}^T\boldsymbol{L}\rangle(1 + \zeta/R)\mathrm{d}\zeta \tag{14c}$$

being $\boldsymbol{I}_{3\times 3}$ the 3×3 identity matrix. Finally, using Eq. (8), the stationarity condition of Π yields the governing equilibrium equations in terms of the problem primary variables, which are the generalized displacements.

3 Ritz Solution

The cylindrical panel model is numerically solved by a Ritz approach [17, 27, 33–35] whose trial functions χ are built basing on the tensor product of one-dimensional polynomials defined over the natural coordinates ξ and η [35]

$$\chi = f_\chi(\xi, \eta)\phi_m(\xi)\,\psi_n(\eta) \tag{15}$$

where $\phi_m(\xi)$ and $\psi_n(\eta)$ are one-dimensional Legendre orthogonal polynomials of order m and n, respectively, and f_χ is the boundary function. The boundary function f_χ can be suitably chosen to ensure zero value of the trial function along selected external edges of the domain and then enables the fulfillment of homogeneous kinematical boundary conditions. In particular, it is defined as

$$f_\chi(\xi, \eta) = (1 + \xi)^{a_1}(1 - \xi)^{a_2}(1 + \eta)^{a_3}(1 - \eta)^{a_4} \tag{16}$$

where the exponents a_i take the value 0 or 1 according to the condition of zero (namely constrained) or unknown value of χ along the edge implicitly described by the corresponding power base, see Table 1.

3.1 Generalized Displacements and Strains Approximation

The shell panel displacements $\boldsymbol{u}$ and $\boldsymbol{\vartheta}$, namely the problem primary variables, are discretized as

$$\tau = \sum_{m=0}^{M^\tau} \sum_{n=0}^{N^\tau} f_{\chi^\tau}(\xi, \eta)\phi_m(\xi)\,\psi_n(\eta)\widetilde{C}_{mn}^\tau \tag{17}$$

where $\tau \in \{u, v, w, \vartheta_x, \vartheta_y\}$ and $\widetilde{C}_{mn}^\tau$ are the unknown Ritz coefficients. To enable an efficient matrix notation, Eq. (17) is rewritten as

$$\tau = \sum_{i=1}^{(M^\tau+1)(N^\tau+1)} \chi_i^\tau C_i^\tau = \boldsymbol{\Psi}_\tau \boldsymbol{C}_\tau \tag{18}$$

where χ_i^τ and C_i^τ are the i–th component of the trial functions row vector $\boldsymbol{\Psi}_\tau$ and the Ritz coefficients column vector $\boldsymbol{C}_\tau$, respectively. The χ_i^τ and C_i^τ components are built based on the following rules

$$\begin{aligned}&\chi_{(n+m[N^\tau+1]+1)}^\tau = f_\chi(\xi, \eta)\phi_m(\xi)\,\psi_n(\eta) \\ &\quad \text{for } m = 0, 1..., M^\tau,\ n = 0, 1..., N^\tau\end{aligned} \tag{19a}$$

Table 1 Possible combination of the exponents in Eq. (16)

Edge	$(1 + \xi) = 0$	$(1 - \xi) = 0$	$(1 + \eta) = 0$	$(1 - \eta) = 0$
Free	$a_1 = 0$	$a_2 = 0$	$a_3 = 0$	$a_4 = 0$
Constrained	$a_1 = 1$	$a_2 = 1$	$a_3 = 1$	$a_4 = 1$

$$C^{\tau}_{(n+m[N^{\tau}+1]+1)} = C^{\tau}_{mn} \quad \text{for } m = 0, 1..., M^{\tau},\ n = 0, 1..., N^{\tau} \tag{19b}$$

The generalized displacement approximations are then collected in compact matrix form as

$$\boldsymbol{u} = \begin{bmatrix} \boldsymbol{\Psi}_u & \boldsymbol{0} & \boldsymbol{0} \\ \boldsymbol{0} & \boldsymbol{\Psi}_v & \boldsymbol{0} \\ \boldsymbol{0} & \boldsymbol{0} & \boldsymbol{\Psi}_w \end{bmatrix} \begin{Bmatrix} \boldsymbol{C}_u \\ \boldsymbol{C}_v \\ \boldsymbol{C}_w \end{Bmatrix} = \boldsymbol{\Phi}_u \boldsymbol{U} \tag{20a}$$

$$\boldsymbol{\vartheta} = \begin{bmatrix} \boldsymbol{\Psi}_{\vartheta_x} & \boldsymbol{0} \\ \boldsymbol{0} & \boldsymbol{\Psi}_{\vartheta_y} \end{bmatrix} \begin{Bmatrix} \boldsymbol{C}_{\vartheta_x} \\ \boldsymbol{C}_{\vartheta_y} \end{Bmatrix} = \boldsymbol{\Phi}_{\vartheta} \boldsymbol{\Theta} \tag{20b}$$

Accordingly, the discretized form of the generalized strain reads as

$$\boldsymbol{\varepsilon} = \mathscr{D}_{pu} \boldsymbol{\Phi}_u \boldsymbol{U} = \mathcal{B}_{pu} \boldsymbol{U} \tag{21a}$$

$$\boldsymbol{\kappa} = \mathscr{D}_{p\vartheta} \boldsymbol{\Phi}_{\vartheta} \boldsymbol{\Theta} = \mathcal{B}_{p\vartheta} \boldsymbol{\Theta} \tag{21b}$$

$$\boldsymbol{\gamma}_0 = \boldsymbol{\Phi}_{\vartheta} \boldsymbol{\Theta} + \mathscr{D}_{nu} \boldsymbol{\Phi}_u \boldsymbol{U} = \boldsymbol{\Phi}_{\vartheta} \boldsymbol{\Theta} + \mathcal{B}_{nu} \boldsymbol{U} \tag{21c}$$

3.2 Discrete Governing Equations

The Ritz discrete kinematics, as defined by Eqs. (16) and (17), is substituted into the energy potential $\boldsymbol{\Pi}$, resulting in its discretized form. By applying variational calculus, the governing equations of the problem are derived in terms of the unknown Ritz coefficients and they are finally expressed as:

$$\left(\boldsymbol{K} - \omega^2 \boldsymbol{M}\right) \boldsymbol{X} = 0 \tag{22}$$

where $\boldsymbol{X} = \left\{ \boldsymbol{U}^T \ \ \boldsymbol{\Theta}^T \right\}^T$ is the vector containing the unknown Ritz coefficients, $\boldsymbol{K}$ represents the stiffness matrix, and $\boldsymbol{M}$ denotes the mass matrix. They are defined by

$$\boldsymbol{M} = \begin{bmatrix} \int_{\Omega_c} \boldsymbol{\Phi}_u^T \boldsymbol{I}_{uu} \boldsymbol{\Phi}_u \mathrm{d}\Omega & \int_{\Omega_c} \boldsymbol{\Phi}_u^T \boldsymbol{I}_{u\vartheta} \boldsymbol{\Phi}_{\vartheta} \mathrm{d}\Omega \\ [1em]\text{symm} & \int_{\Omega_c} \boldsymbol{\Phi}_{\vartheta}^T \boldsymbol{I}_{\vartheta\vartheta} \boldsymbol{\Phi}_{\vartheta} \mathrm{d}\Omega \end{bmatrix} \tag{23}$$

$$\boldsymbol{K} = \begin{bmatrix} \int_{\Omega_c} \left[\mathbf{B}_{pu}^T \boldsymbol{A} \mathbf{B}_{pu} + \mathbf{B}_{nu}^T \boldsymbol{A}_S \mathbf{B}_{nu} \right] \mathrm{d}\Omega & \int_{\Omega_c} \left[\mathbf{B}_{pu}^T \boldsymbol{B} \mathbf{B}_{p\vartheta} + \mathbf{B}_{nu}^T \boldsymbol{A}_S \boldsymbol{L} \boldsymbol{\Phi}_{\vartheta} \right] \mathrm{d}\Omega \\ [1em]\text{symm} & \int_{\Omega_c} \left[\mathbf{B}_{p\vartheta}^T \boldsymbol{D} \mathbf{B}_{p\vartheta} + \boldsymbol{\Phi}_{\vartheta}^T \boldsymbol{L}^T \boldsymbol{A}_S \boldsymbol{L} \boldsymbol{\Phi}_{\vartheta} \right] \mathrm{d}\Omega \end{bmatrix} \tag{24}$$

Equation (22) represents a linear algebraic eigenvalue problem whose solution yields the natural circular frequencies of the panel and the corresponding Ritz coefficients, which allow for the reconstruction of the modal shapes.

4 Structural Operators Computation

The computation of the mass and stiffness matrices involves evaluating complex domain integrals which requires the use of appropriate numerical integration techniques. In this work, we employ high-order quadrature rules, developed using the algorithm presented in Ref. [36], which leverage the implicit description of the cutout via a level set function. These quadrature rules are further enhanced with an adaptive subregioning scheme to improve integration accuracy and efficiency.

According with the geometrical description introduced in Sect. 2, the points $\boldsymbol{P}$ of the panel mid-surface Ω_c map into the subdomain $\widetilde{\Omega}_c$ of the natural coordinate square domain Q, as illustrated in Fig. 3.

Thus, the integral of a generic function $f(\boldsymbol{P})$ over Ω_c can be expressed as:

$$\int_{\Omega_c} f(\boldsymbol{P}) \mathrm{d}\Omega = \int_{\widetilde{\Omega}_c} f[\boldsymbol{P}(\xi, \eta)] J(\xi, \eta) \mathrm{d}\Omega, \tag{25}$$

where $J(\xi, \eta)$ is the determinant of the Jacobian matrix of the mapping. The numerical evaluation of the integral on the right-hand side of Eq. (25) is accomplished as:

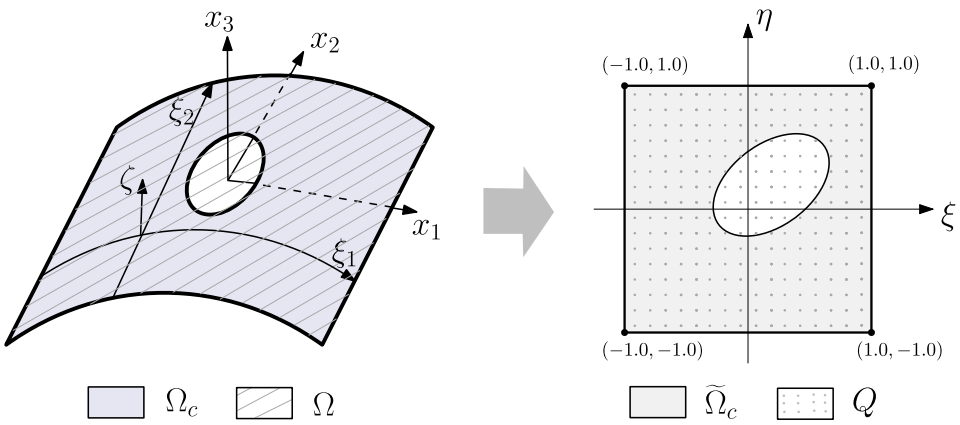

Fig. 3 Mapping of a cylindrical panel with a *cutout*

$$\int_{\widetilde{\Omega}_s} f[\boldsymbol{P}(\xi,\eta)]J(\xi,\eta)\mathrm{d}\Omega = \sum_{g=1}^{N_g} f^g J^g w^g, \tag{26}$$

f^g is the value of the function f evaluated at the integration point with natural coordinates (ξ^g, η^g), J^g is the value of $J(\xi,\eta)$ at the integration point, w^g is the weight associated with the integration point, and N_g is the total number of integration points, namely the quadrature order. The set of integration points and their weights defines the *quadrature rule* for the domain $\widetilde{\Omega}_c$.

4.1 Panel Without *Cutout*

For panels without a cutout, the integration domain Ω_c corresponds to the entire panel domain Ω; consequently, the $\widetilde{\Omega}_c$ domain coincides with the entire natural coordinates square domain Q. In this case, the integration points and weights are determined by the tensor product of the standard one-dimensional Gauss quadrature rules.

4.2 Panel with *Cutout*

The domain Ω_c is defined using a *level set* function φ, as described by Eq. (2). This function can be expressed in terms of the natural coordinates (ξ,η) by introducing an auxiliary *level set* function $\widetilde{\varphi}$ defined over the square domain Q such that:

$$\widetilde{\varphi}(\xi,\eta) \equiv \varphi(\boldsymbol{P}(\xi,\eta)). \tag{27}$$

It is worth noting that, in this way, the auxiliary *level set* function defines the $\widetilde{\Omega}_c$ integration domain in the natural variables (ξ,η), enabling the application of the algorithm for computing quadrature rules on implicitly defined domains, developed in Refs. [36–38].

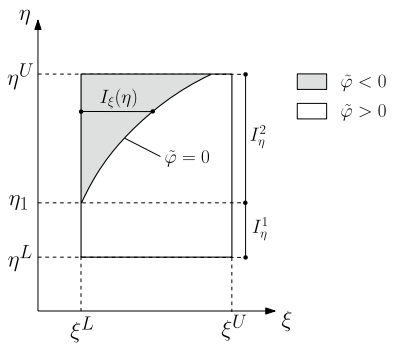

Fig. 4 Example case of integration over a domain Q_k that intersects the boundary of $\widetilde{\varphi}$: geometrical sketch

The algorithm begins by partitioning the square domain Q into subdomains, ensuring each satisfies one of the following conditions:

a) $\widetilde{\varphi}$ is always negative within the subdomain;

b) $\widetilde{\varphi}$ is always positive within the subdomain;

c) $\widetilde{\varphi}$ changes sign, but its gradient $\partial\widetilde{\varphi}/\partial\xi$ in the ξ direction or $(\partial\widetilde{\varphi}/\partial\eta)$ in the η direction maintains a consistent sign.

The partitioning starts from Q and is performed recursively:

i) If none of the conditions (*a*, *b*, or *c*) are met, Q is divided into two subdomains Q_1 and Q_2. The subdivision direction is chosen based on the smaller gradient magnitude of $\widetilde{\varphi}$.

ii) The process is repeated for Q_1 and Q_2 until all subdomains satisfy one of the specified conditions.

Once the partitioning of the Q domain is established, for each subdomain Q_k, the integration rules are determine according to the following cases:

- If Q_k lies entirely outside the *cutout* and within the panel domain, the integration points and weights are computed using the tensor product of one-dimensional Gauss quadrature rules.
- If Q_k lies entirely within the *cutout* (outside the panel domain), the subdomain does not contribute to the integrals, so its integration points and weights are empty.
- If Q_k intersects the boundary of $\widetilde{\varphi}$, special quadrature is established; it rests on the consistent gradient sign in $Q_k \equiv [\xi^L, \xi^U] \times [\eta^L, \eta^U]$, which ensures that $\widetilde{\varphi}$ has at most one zero along ξ or η for a fixed coordinate. The integration process involves the following steps:

  (1) Compute all zeros of $\widetilde{\varphi}(\xi = \xi^L, \eta)$ and $\widetilde{\varphi}(\xi = \xi^U, \eta)$.
  (2) Create an ordered list of η values, starting with η^L and ending with η^U. Interior values correspond to the computed zeros. Denote the list as $\{\eta_0, \ldots, \eta_{n+1}\}$, where $\eta_0 = \eta^L$ and $\eta_{n+1} = \eta^U$.
  (3) Define intervals $I_\eta^i = [\eta_{i-1}, \eta_i]$ for $i = 1, \ldots, n+1$.
  (4) The integral of a generic function f over Q_k is given by:

Table 2 Convergence of the non-dimensional frequency parameter $\bar{\omega}_i$ of the first four free vibration modes of the isotropic panels

		Without cutout				With cutout			
	Approx	$\bar{\omega}_1$	$\bar{\omega}_2$	$\bar{\omega}_3$	$\bar{\omega}_4$	$\bar{\omega}_1$	$\bar{\omega}_2$	$\bar{\omega}_3$	$\bar{\omega}_4$
$R = \infty$	S_4	2.999	145.897	145.897	206.316	5.507	165.794	165.794	221.704
	S_8	2.998	6.116	6.116	9.017	5.474	7.101	7.101	9.520
	S_{12}	2.998	6.114	6.114	9.014	5.460	6.609	6.609	9.077
	S_{16}	2.998	6.114	6.114	9.014	5.455	6.497	6.497	8.986
	S_{20}	2.998	6.114	6.114	9.014	5.452	6.448	6.448	8.943
	S_{24}	2.998	6.114	6.114	9.014	5.450	6.422	6.422	8.853
	S_{28}	2.998	6.114	6.114	9.014	5.449	6.404	6.406	8.780
	S_{32}	2.998	6.114	6.114	9.014	5.449	6.395	6.396	8.731
	Ref. [39]	3.021	6.201	6.218	9.234	5.511	6.491	6.549	9.026
	Ref. [16]	2.997	6.111	6.111	9.009	5.460	6.370	6.374	8.558
	FEM	2.999	6.126	6.128	9.029	5.444	6.352	6.352	8.548
$R = 2$	S_4	15.666	145.447	146.709	206.297	18.332	165.310	166.637	221.508
	S_8	9.248	10.523	14.117	14.466	10.134	10.802	13.829	15.305
	S_{12}	9.239	10.501	14.099	14.449	8.913	9.329	13.169	14.243
	S_{16}	9.239	10.501	14.099	14.449	8.486	8.700	12.989	13.814
	S_{20}	9.239	10.501	14.099	14.449	8.295	8.462	12.900	13.632
	S_{24}	9.239	10.501	14.099	14.449	8.193	8.345	12.844	13.539
	S_{28}	9.239	10.501	14.099	14.449	8.128	8.269	12.808	13.477
	S_{32}	9.239	10.501	14.099	14.449	8.082	8.217	12.783	13.437
	Ref. [39]	9.415	10.776	14.211	14.605	8.552	8.742	13.116	14.153
	Ref. [16]	9.246	10.534	14.104	14.465	7.899	8.022	12.678	13.330
	FEM	9.243	10.532	14.101	14.463	7.893	8.010	12.660	13.273

Table 3 Convergence of the non-dimensional frequency parameter $\bar{\omega}_i$ of the first four free vibration modes of the simply-supported, $[0/90]_4$ layup cross-ply cylindrical panel with central square cutout

	Approx.	$\bar{\omega}_1$	$\bar{\omega}_2$	$\bar{\omega}_3$	$\bar{\omega}_4$
c/a = 0.0	S_4	7.583	14.482	19.016	21.119
	S_8	7.556	12.016	16.929	17.600
	S_{12}	7.556	12.015	16.929	17.599
	S_{16}	7.556	12.015	16.929	17.599
	S_{20}	7.556	12.015	16.929	17.599
	S_{24}	7.556	12.015	16.929	17.599
	S_{28}	7.556	12.015	16.929	17.599
	S_{32}	7.556	12.015	16.929	17.599
	Ref. [40]	7.543	–	–	–
c/a = 0.3	S_4	8.542	14.776	19.388	20.999
	S_8	8.281	11.874	17.061	17.096
	S_{12}	7.995	11.248	16.650	16.903
	S_{16}	7.915	10.623	16.224	16.708
	S_{20}	7.875	10.422	16.085	16.640
	S_{24}	7.857	10.315	16.009	16.611
	S_{28}	7.846	10.242	15.956	16.585
	S_{32}	7.836	10.200	15.926	16.573
	Ref. [40]	7.816	–	–	–
c/a = 0.5	S_4	10.577	16.374	21.446	22.000
	S_8	9.038	10.313	16.275	17.029
	S_{12}	8.563	8.769	15.323	15.831
	S_{16}	8.424	8.443	15.170	15.573
	S_{20}	8.300	8.342	15.108	15.457
	S_{24}	8.211	8.293	15.069	15.380
	S_{28}	8.145	8.276	15.046	15.324
	S_{32}	8.118	8.242	15.034	15.299
	Ref. [40]	8.172	–	–	–

$$\int_{Q_k} f(\xi,\eta)\,d\xi d\eta = \sum_{i=1}^{n+1} \int_{I_\eta^i} \hat{f}(\eta)\,d\eta, \tag{28}$$

where

$$\hat{f}(\eta) \equiv \int_{I_\xi(\eta)} f(\xi,\eta)\,\mathrm{d}\xi. \tag{29}$$

The interval $I_\xi(\eta)$ depends on the zeros of $\widetilde{\varphi}$:

(4.1) If $\partial\widetilde{\varphi}/\partial\xi > 0$, $I_\xi(\eta) = [\xi^L, \xi_k]$, where ξ_k is the zero.

(4.2) If $\partial\widetilde{\varphi}/\partial\xi < 0$, $I_\xi(\eta) = [\xi_k, \xi^U]$.

(4.3) If $\widetilde{\varphi}$ has no zeros, $I_\xi(\eta) = [\xi^L, \xi^U]$.

Using one-dimensional Gauss quadrature for each interval I_η^i and the corresponding $I_\xi(\eta)$, the integration points and weights for Q_k are computed.

Figure 4 shows the geometrical sketch for an exemplificative case of integration over a domain Q_k that intersects the boundary of $\widetilde{\varphi}$.

Table 4 [0/90/90/0] laminated cylindrical panel having square planform with edge length $L = 0.4$ m, a central circular cutout with radius $R = 0.25$ m and different edge constraints (CCCC, SSSS, CFFF): frequencies $\omega/2\pi$ of the first six natural modes

	CCCC			SSSS			CFFF		
Mode	Present	FEM	Error %	Present	FEM	Error %	Present	FEM	Error %
1	978.9	976.7	0.23%	850.2	849.8	0.05%	145.3	145.1	0.11%
2	1098.2	1096.4	0.17%	884.1	882.5	0.17%	162.1	162.1	0.07%
3	1355.7	1353.9	0.13%	1087.5	1086.6	0.08%	398.1	397.3	0.22%
4	1399.6	1393.3	0.45%	1188.0	1183.8	0.35%	398.1	397.4	0.18%
5	1503.9	1500.8	0.21%	1239.2	1237.1	0.17%	530.2	529.9	0.06%
6	1526.2	1519.6	0.43%	1339.3	1333.8	0.41%	555.2	555.2	0.02%

Table 5 Fully clamped (CCCC) cylindrical panel having square planform with edge length $L = 0.4$ m, a central circular cutout with radius $R = 0.25$ m and different layups: frequencies $\omega/2\pi$ of the first six natural modes

	[90/0/0/90]			[0/45/-45/90]			$[0/45/-45/90]_S$		
	Present	FEM	Error %	Present	FEM	Error %	Present	FEM	Error %
1	977.5	976.7	0.09%	1312.6	1312.2	0.02%	1895.4	1897.0	−0.08%
2	1097.2	1096.4	0.07%	1396.6	1384.6	0.87%	2260.8	2267.3	−0.29%
3	1354.1	1353.9	0.01%	1566.7	1563.1	0.23%	2417.4	2428.7	−0.47%
4	1394.5	1393.4	0.09%	1662.4	1649.0	0.81%	2794.4	2802.2	−0.28%
5	1502.1	1500.8	0.08%	1684.8	1672.7	0.72%	3004.7	3018.4	−0.45%
6	1521.2	1519.6	0.10%	1763.4	1740.5	1.32%	3268.9	3282.7	−0.42%

Table 6 Free vibrations frequencies $\omega/2\pi$ for the $[0/45/-45/90]_S$, fully clamped, cylindrical panel with different cutouts

Geometry	Mode	1	2	3	4	5	6
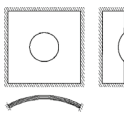	Present	1895.38	2260.8	2417.4	2794.44	3004.69	3268.88
	FEM	1896.97	2267.32	2428.7	2802.24	3018.37	3282.73
	error	-0.08%	-0.29%	-0.47%	-0.28%	-0.45%	-0.42%
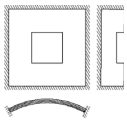	Present	1723.81	1875.64	2454.01	2850.15	2896.46	3060.07
	FEM	1720.31	1889.33	2449.24	2795.24	2878	3067.71
	error	0.20%	-0.72%	0.19%	1.96%	0.64%	-0.25%
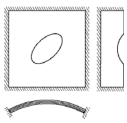	Present	1910.66	2390.98	2537.73	2703.57	2887.07	3346.23
	FEM	1910.81	2390.19	2546.32	2707.7	2895.67	3357.06
	error	-0.01%	0.03%	-0.34%	-0.15%	-0.30%	-0.32%
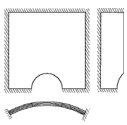	Present	1754.68	2281.8	2728.39	2950.26	3439.18	3499.5
	FEM	1760.41	2287.37	2740.65	2961.71	3448.41	3513.82
	error	-0.33%	-0.24%	-0.45%	-0.39%	-0.27%	-0.41%

5 Method Validation

A computer code has been implemented to validate the formulation described in the previous sections.

5.1 Convergence Analysis

Preliminarily, convergence studies are presented and discussed comparing the present results with those available in the literature [16, 39, 40] or from finite element solutions obtained by ABAQUS using S3R and S4R shell-type elements. Both isotropic and laminated structures, with and without cutouts, were analyzed. Trial functions are chosen as in Eq. (15), with m and n ranging over the set $\{1, 2, ..., N\}$

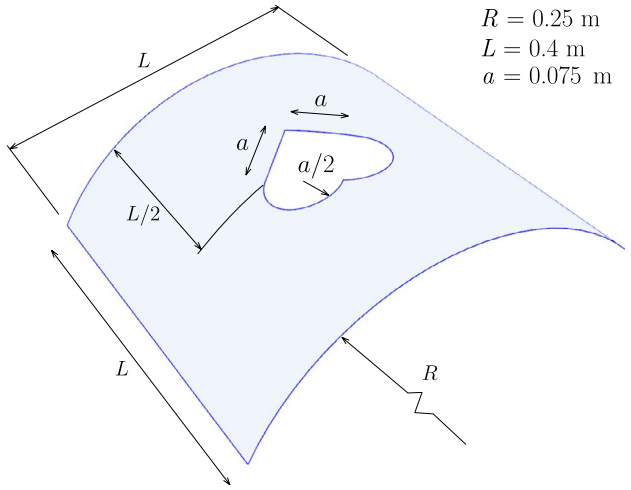

Fig. 5 Cylindrical panel with a centered heart-shaped cutout: geometry and dimensions

and the same approximation order N was applied to all primary variables. This approximation scheme is denoted as S_N. Results are presented using the mode non-dimensional frequency parameter $\bar{\omega}_i = \omega_i L^2 \sqrt{\left[\rho\left(1-\nu_{12}^2\right)\right]\left(12E_2h^2\right)}$.

The first case examines a clamped, isotropic aluminum panel. The panel configurations have square planform geometry with edge length $L = 0.5$ m, thickness $h = 2$ mm, and two values for the cylinder radius, $R = \{\infty, 2\,\text{m}\}$. A central square cutout with edge length $c = 0.25$ m has been considered and the material properties have been set as $E = 68.796$ GPa, $\nu = 0.3$ and $\rho = 2720\,\text{kg/m}^3$. The natural frequencies for the isotropic panel configurations, both with and without the central cutout, are provided in Table 2. The reported FEM results were obtained using elements with a characteristic length of $0.0625L$ that was determined through convergence studies and that, for the considered cases, gives convergent values of the first four vibration frequencies with a maximum relative error on the order of 0.5 %.

The second case involves a simply-supported, cross-ply cylindrical panel with a $[0/90]_4$ layup. The panel has a square planform with edge length L, a thickness ratio of $L/h = 100$, and a cylinder radius of $R/h = 300$. A central square cutout with varying edge lengths $c/a = 0$, 0.3, 0.5 has been considered and the material properties for the plies are given as $E_1 = 25E_2, G_{12} = G_{13} = 0.5E_2, G_{23} = 0.2E_2$ and $\nu_{12} = 0.25$. The results for the natural frequencies under these conditions are summarized in Table 3.

The results of the proposed studies, which are representative of many other cases analyzed and not reported here for brevity, demonstrate excellent convergence properties for the proposed method. It is observed that convergence for cut panels is slower, which can be attributed to the complex geometry that requires more terms in the approximation of the primary variables.

5.2 Method Accuracy

To ascertain the method accuracy with respect to different panel configurations, analyses have been carried out for a multilayered cylindrical shell panel having radius $R = 0.25$ m and a square planform with edge length $L = 0.4$ m. The ply thickness and material properties are set as $t = 0.002$ m, $E_1 = 113.0$ GPa, $E_2 = 9.0$ GPa $\nu_{12} = 0.302$, $G_{23} = G_{13} = G_{12} = 3.82$ GPa and $\rho = 1540.0\,\text{kg/m}^3$. Different boundary conditions, layups, and cutout shapes have been considered, and the results compared with finite element solutions obtained using elements with a characteristic length of $0.0625L$ that was determined through convergence studies and that, for the considered cases, gives convergent values of the first six vibration frequencies with a maximum relative error on the order of 1.0%. Table 4 lists the free vibration frequencies ($\omega/2\pi$ [Hz]) of the [0/90/90/0] composite cylindrical with different edges kinematical constraints. As usual, the edge kinematical constraint type is denoted by the letters C, S, and F standing for clamped, simply supported, and free, whereas the panel constraint configuration is described by four letters each associated with an edge, starting from the $x_2 = -L$ edge and proceeding in a counterclockwise direction.

The comparison of the present results with those of converged finite element analyses shows the accuracy of the present solution with respect to different kinematical boundary conditions. Table 5 lists the free vibration frequencies ($\omega/2\pi$ [Hz]) of the fully clamped panel with different stacking sequences, namely a four ply cross-ply layup, a four ply non symmetric layup, and an eight ply symmetric layup. The results obtained show very good agreement with the reference solutions and validate the method accuracy with respect to the layup parameters.

To illustrate the method's capability in dealing with different cutout shapes and positions, Table 6 reports the frequencies $\omega_i/2\pi$ for the clamped cylindrical panel with $[0/45/–45/90]_S$ layup and different cutouts. Analyses refer to a central circular cutout with radius $r = 0.075$ m; an edge semicircular cutout with radius $r = 0.075$ m, a central square cutout with edge length $a = 0.075$ m and a central, 45° inclined, elliptical cutout with axes length $a = 0.15$ m and $b = 0.075$ m. For a geometrical sketch of the investigated cutouts, refer to the first column of Table 6. The presented results have been obtained by the S_{24} discretization scheme, providing solutions that can be considered converged. In all the investigated cases, the agreement between the present and the reference solutions is very good with low percentage errors. It is worth noting some discrepancies for the square cutout cases which, however, are contained below

Mode	Frequency [Hz]		
	Ritz	FEM	% error
1	1908.8	1914.6	0.31%

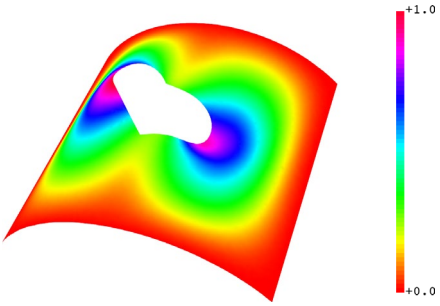

Mode	Frequency [Hz]		
	Ritz	FEM	% error
2	2489.4	2465.3	-0.97%

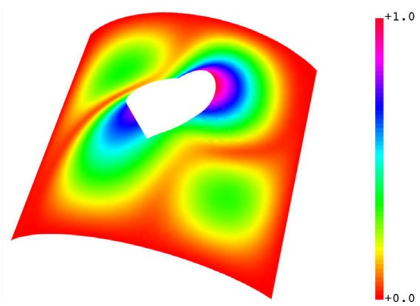

Mode	Frequency [Hz]		
	Ritz	FEM	% error
3	2563.2	2548.1	-0.59%

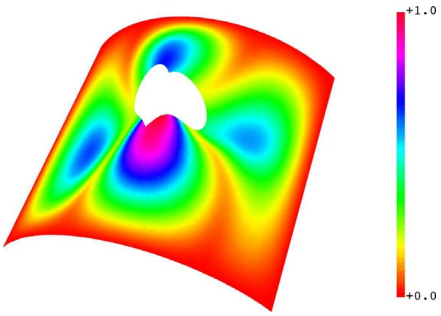

Mode	Frequency [Hz]		
	Ritz	FEM	% error
4	2593.3	2619.7	1.02%

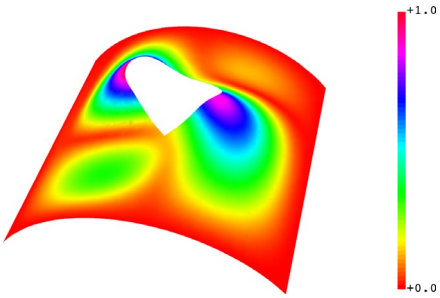

Mode	Frequency [Hz]		
	Ritz	FEM	% error
5	2947.8	2974.6	0.91%

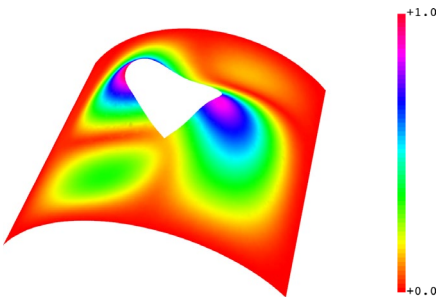

Mode	Frequency [Hz]		
	Ritz	FEM	% error
6	3390.8	3377.3	-0.40%

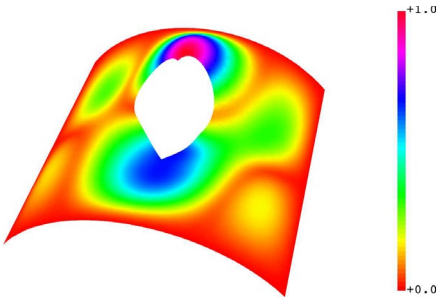

Fig. 6 Modes frequency and shape for the $[0/45/–45/90]_S$ fully clamped cylindrical panel with a centered heart-shaped cutout. The colored maps represent the normalized displacement magnitude

2%. Table 6 shows the computed modal shape for the investigated cases illustrating the ability of the proposed method in capturing the panel behavior.

The last application illustrates the capability of the proposed approach in dealing with complex cutout shapes. To this aim a centered, heart-shaped cutout is considered for the $[0/45/–45/90]_S$, fully clamped, cylindrical panel. The relevant dimensions of the considered panel are shown in Fig. 5, whereas the implicit function used to describe the heart-shaped cutout is given in Appendix 7.

Figure 6 shows the results obtained with the S_{24} approximation scheme in terms of free vibration frequencies and the corresponding modal shapes; comparison is reported with the finite elements solution; this was obtained by a FEM model with 26,922 elements, 27,224 nodes, and 163,344 dofs, which provides converged values of the first

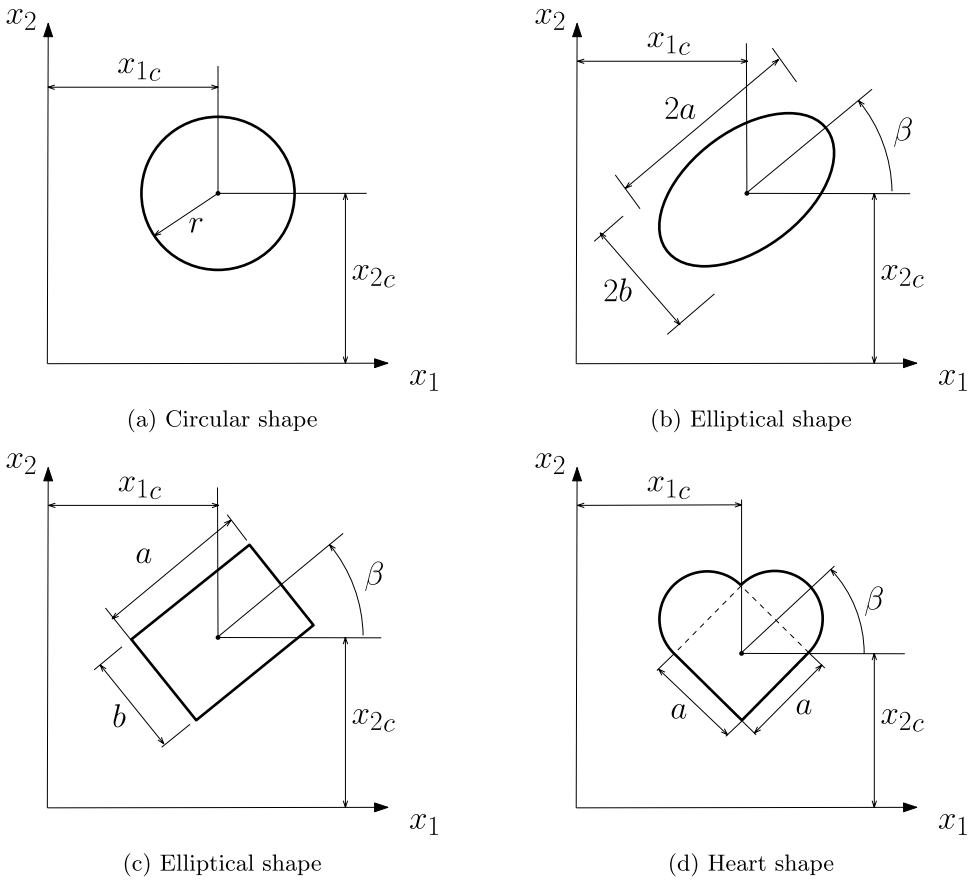

(a) Circular shape (b) Elliptical shape

(c) Elliptical shape (d) Heart shape

Fig. 7 Geometrical parameters for the level set functions describing the cutouts

six vibration frequencies with a maximum relative error lower than 1.0%. Also, in this complex cutout case, the results are in good agreement with finite elements, confirming the capabilities and effectiveness of the proposed approach.

6 Conclusion

A single-domain Ritz method has been presented for analyzing the free vibrations of laminated composite cylindrical panels with cutouts. This method is based on the first-order shear deformation theory, where the reference domain of the panel is implicitly defined using a level set function, allowing for the use of an efficient quadrature algorithm to compute the stiffness and mass matrices. The convergence and accuracy of the proposed method have been thoroughly studied and assessed. Furthermore, the method ability to handle different edge constraints, layup configurations, and cutout shapes has been investigated. The results from all conducted tests demonstrate a strong alignment with reference solutions available in the literature or obtained from finite element analysis, confirming that the proposed approach is an effective tool for analyzing the free vibrations of cylindrical panels with cutouts of various shapes.

Level Set Functions for the Cutouts

Four cutout shapes are considered: circular, elliptical, rectangular, and heart-shaped. The cutout is defined through the geometrical parameters shown in Fig. 7. The associated *level set* functions can be expressed as follows:

– circular shape

$$\varphi_1(x_{1c}, x_{2c}, r) = r^2 - (x_1 - x_{1c})^2 - (x_2 - x_{2c})^2 \tag{30}$$

– elliptical shape

$$\varphi_2(x_{1c}, x_{2c}, a, b, \beta) = 1 - \left(\frac{\tilde{x}_1}{a}\right)^2 - \left(\frac{\tilde{x}_2}{b}\right)^2 \tag{31}$$

– rectangular shape

$$\varphi_3(x_{1c}, x_{2c}, w, h, \beta) = \frac{1}{2}wh - \left|\frac{1}{2}h\tilde{x}_1 - \frac{1}{2}w\tilde{x}_2\right| - \left|\frac{1}{2}h\tilde{x}_1 + \frac{1}{2}w\tilde{x}_2\right| \tag{32}$$

– heart shape

$$\varphi_4(x_{1c}, x_{2c}, a, \beta) = 1 - \left[\max\left(0, 1 - \frac{\varphi_3(x_{1c}, x_{2c}, a, a, \beta)}{\delta_1}\right)\right]^{\delta_2} - \left[\max\left(0, 1 - \frac{\varphi_1(a\cos\beta, -a\sin\beta, a/2)}{\delta_1}\right)\right]^{\delta_2} - \left[\max\left(0, 1 - \frac{\varphi_1(a\sin\beta, a\cos\beta, a/2)}{\delta_1}\right)\right]^{\delta_2} \tag{33}$$

where $\delta_1 = 0.001$, $\delta_2 = 2$ [41] and

$$\tilde{x}_1 = (x_1 - x_{1c})\cos\beta + (x_2 - x_{2c})\sin\beta \tag{34a}$$

$$\tilde{x}_2 = -(x_1 - x_{1c})\sin\beta + (x_2 - x_{2c})\cos\beta \tag{34b}$$

Acknowledgements AM acknowledges the support by the European Union-Next Generation EU-National Sustainable Mobility Center CN00000023, Italian Ministry of University and Research-Decree n.1033-17/06/2022, Spoke 12, CUP B73C22000760001.

Funding Open access funding provided by Università degli Studi di Palermo within the CRUI-CARE Agreement.

Data availability Data will be made available on request.

References

1. Carrera, E., Zappino, E.: Carrera unified formulation for free-vibration analysis of aircraft structures. AIAA J. **54**(1), 280–292 (2016)
2. Petrolo, M., Carrera, E.: Best spatial distributions of shell kinematics over 2d meshes for free vibration analyses. Aerotecnica Missili & Spazio **99**, 217–232 (2020)
3. Noor, A.K., Burton, W.S.: Assessment of computational models for multilayered composite shells (1990)
4. Qatu, M.S.: Recent research advances in the dynamic behavior of shells: 1989–2000, part 1: Laminated composite shells. Appl. Mech. Rev. **55**(4), 325–350 (2002)
5. Qatu, M.S.: Vibration of Laminated Shells and Plates. Elsevier (2004)
6. Qatu, M.S., Sullivan, R.W., Wang, W.: Recent research advances on the dynamic analysis of composite shells: 2000–2009. Compos. Struct. **93**(1), 14–31 (2010)
7. Jin, G., Ye, T., Su, Z.: Structural Vibration: A Uniform Accurate Solution for Laminated Beams, Plates and Shells with General Boundary Conditions. Springer, Berlin, Heidelberg (2015). https://doi.org/10.1007/978-3-662-46364-2
8. Bicos, A.S., Springer, G.S.: Vibrational characteristics of composite panels with cutouts. AIAA J. **27**(8), 1116–1122 (1989)
9. Sahu, S., Datta, P.: Dynamic stability of laminated composite curved panels with cutouts. J. Eng. Mech. **129**(11), 1245–1253 (2003)
10. Nanda, N., Bandyopadhyay, J.: Nonlinear free vibration analysis of laminated composite cylindrical shells with cutouts. J. Reinf. Plast. Compos. **26**(14), 1413–1427 (2007)
11. Chaubey, A.K., Kumar, A., Chakrabarti, A.: Vibration of laminated composite shells with cutouts and concentrated mass. AIAA J. **56**(4), 1662–1678 (2018)
12. Poore, A., Barut, A., Madenci, E.: Free vibration of laminated cylindrical shells with a circular cutout. J. Sound Vib. **312**(1–2), 55–73 (2008)
13. Dey, S., Mukhopadhyay, T., Sahu, S., Adhikari, S.: Effect of cutout on stochastic natural frequency of composite curved panels. Compos. B Eng. **105**, 188–202 (2016)
14. Kurpa, L., Timchenko, G., Osetrov, A., Shmatko, T.: Nonlinear vibration analysis of laminated shallow shells with clamped cutouts by the r-functions method. Nonlinear Dyn. **93**, 133–147 (2018)
15. Kwak, S., Kim, K., Yun, J., Kim, S., Ri, P.: Free vibration analysis of laminated closed conical, cylindrical shells and annular plates with a hole using a meshfree method. Structures **34**(3), 3070–3086 (2021). https://doi.org/10.1016/j.istruc.2021.09.057
16. Talezadehlari, A.: Free vibration analysis of perforated composite cylindrical shell and panel using multi-domain generalized differential quadrature (gdq) method. Compos. Struct. **287**, 115337 (2022)
17. Ilanko, S., Monterrubio, L., Mochida, Y.: The Rayleigh-Ritz Method for Structural Analysis. Wiley, Hoboken (2014)
18. Qatu, M.S., Leissa, A.W.: Free vibrations of completely free doubly curved laminated composite shallow shells. J. Sound Vib. **151**(1), 9–29 (1991)
19. Qatu, M.S., Leissa, A.W.: Natural frequencies for cantilevered doubly-curved laminated composite shallow shells. Compos. Struct. **17**(3), 227–255 (1991)
20. Raouf, R.A., Palazotto, A.N.: Non-linear free vibrations of symmetrically laminated, slightly compressible cylindrical shell panels. Compos. Struct. **20**(4), 249–257 (1992)
21. Awrejcewicz, J., Kurpa, L., Shmatko, T.: Linear and nonlinear free vibration analysis of laminated functionally graded shallow shells with complex plan form and different boundary conditions. Int. J. Non-Linear Mech. **107**, 161–169 (2018)
22. Soldatos, K., Messina, A.: Vibration studies of cross-ply laminated shear deformable circular cylinders on the basis of orthogonal polynomials. J. Sound Vib. **218**(2), 219–243 (1998)
23. Jin, G., Ye, T., Chen, Y., Su, Z., Yan, Y.: An exact solution for the free vibration analysis of laminated composite cylindrical shells with general elastic boundary conditions. Compos. Struct. **106**, 114–127 (2013)
24. Wang, Q., Shao, D., Qin, B.: A simple first-order shear deformation shell theory for vibration analysis of composite laminated open cylindrical shells with general boundary conditions. Compos. Struct. **184**, 211–232 (2018)
25. Lam, K., Loy, C.: Influence of boundary conditions and fibre orientation on the natural frequencies of thin orthotropic laminated cylindrical shells. Compos. Struct. **31**(1), 21–30 (1995)
26. Sciascia, G., Oliveri, V., Milazzo, A., Weaver, P.M.: Ritz solution for transient analysis of variable-stiffness shell structures. AIAA J. **58**(4), 1796–1810 (2020)
27. Benedetti, I., Gulizzi, V., Milazzo, A.: X-ritz solution for nonlinear free vibrations of plates with embedded cracks. Aerotecnica Missili & Spazio **98**, 75–83 (2019)

28. Kurpa, L., Shmatko, T., Timchenko, G.: Free vibration analysis of laminated shallow shells with complex shape using the r-functions method. Compos. Struct. **93**(1), 225–233 (2010)
29. Zuo, P., Shi, X., Ge, R., Luo, J.: Unified series solution for thermal vibration analysis of composite laminated joined conical-cylindrical shell with general boundary conditions. Thin-Walled Struct. **178**, 109525 (2022)
30. Shi, X., Zuo, P., Zhong, R., Guo, C., Wang, Q.: Thermal vibration analysis of functionally graded conical-cylindrical coupled shell based on spectro-geometric method. Thin-Walled Struct. **175**, 109138 (2022)
31. Zhang, Y., Shi, D.: Vibration analysis of laminated composite coupled double cylindrical shell-annular-rectangular plate system. Compos. Struct. **281**, 115020 (2022)
32. Reddy, J.N.: Mechanics of Laminated Composite Plates and Shells: Theory and Analysis. CRC Press, Boca Raton (2003)
33. Milazzo, A.: Free vibrations analysis of cracked variable stiffness composite plates by the extended ritz method. Mech. Adv. Mater. Struct. **30**(8), 1675–1691 (2023)
34. Milazzo, A., Oliveri, V.: Post-buckling analysis of cracked multilayered composite plates by pb-2 rayleigh-ritz method. Compos. Struct. **132**, 75–86 (2015)
35. Milazzo, A., Guarino, G., Gulizzi, V.: Buckling and post-buckling of variable stiffness plates with cutouts by a single-domain ritz method. Thin-Walled Struct. **182**, 110282 (2023)
36. Saye, R.I.: High-order quadrature methods for implicitly defined surfaces and volumes in hyperrectangles. SIAM J. Sci. Comput. **37**(2), 993–1019 (2015)
37. Gulizzi, V., Benedetti, I., Milazzo, A.: An implicit mesh discontinuous Galerkin formulation for higher-order plate theories. Mech. Adv. Mater. Struct. **27**(17), 1494–1508 (2020)
38. Gulizzi, V., Benedetti, I., Milazzo, A.: A high-resolution layerwise discontinuous Galerkin formulation for multilayered composite plates. Compos. Struct. **242**, 112137 (2020)
39. Fazilati, J., Ovesy, H.: Finite strip dynamic instability analysis of perforated cylindrical shell panels. Compos. Struct. **94**(3), 1259–1264 (2012)
40. Nanda, N., Bandyopadhyay, J.: Large amplitude free vibration of laminated composite shells with cutout. Aircr. Eng. Aerosp. Technol. **80**(2), 165–174 (2008)
41. Gulizzi, V., Saye, R.: Modeling wave propagation in elastic solids via high-order accurate implicit-mesh discontinuous Galerkin methods. Comput. Methods Appl. Mech. Eng. **395**, 114971 (2022)